AFRL-RX-WP-TP-2011-4292

MICROSTRUCTURE AND ROOM TEMPERATURE PROPERTIES OF A HIGH-ENTROPY TaNbHfZrTi ALLOY (PREPRINT)

O.N. Senkov, J.M. Scott, and S.V. Senkova

UES, Inc.

D.B. Miracle and C.F. Woodward

Metals Branch
Metals, Ceramics, and NDE Division

JULY 2011

AIR FORCE RESEARCH LABORATORY
MATERIALS AND MANUFACTURING DIRECTORATE
WRIGHT-PATTERSON AIR FORCE BASE, OH 45433-7750
AIR FORCE MATERIEL COMMAND
UNITED STATES AIR FORCE

REPORT DOCUMENTATION PAGE

Form Approved
OMB No. 0704-0188

1. REPORT DATE *(DD-MM-YY)*	2. REPORT TYPE	3. DATES COVERED *(From - To)*
July 2011	Journal Article Preprint	01 July 2011 – 01 July 2011

4. TITLE AND SUBTITLE
MICROSTRUCTURE AND ROOM TEMPERATURE PROPERTIES OF A HIGH-ENTROPY TaNbHfZrTi ALLOY (PREPRINT)

5a. CONTRACT NUMBER
In-house

5b. GRANT NUMBER

5c. PROGRAM ELEMENT NUMBER
62102F

6. AUTHOR(S)
D.B. Miracle and C.F. Woodward (AFRL/RXLM)
O.N. Senkov, J.M. Scott, and S.V. Senkova (UES, Inc.)

5d. PROJECT NUMBER
4347

5e. TASK NUMBER
20

5f. WORK UNIT NUMBER
LM10512P

7. PERFORMING ORGANIZATION NAME(S) AND ADDRESS(ES)

Metals Branch (AFRL/RXLM)
Metals, Ceramics, and NDE Division
Air Force Research Laboratory, Materials and Manufacturing Directorate
Wright-Patterson Air Force Base, OH 45433-7750
Air Force Materiel Command, United States Air Force

UES, Inc.
Dayton, OH 45432

8. PERFORMING ORGANIZATION REPORT NUMBER
AFRL-RX-WP-TP-2011-4292

9. SPONSORING/MONITORING AGENCY NAME(S) AND ADDRESS(ES)
Air Force Research Laboratory
Materials and Manufacturing Directorate
Wright-Patterson Air Force Base, OH 45433-7750
Air Force Materiel Command
United States Air Force

10. SPONSORING/MONITORING AGENCY ACRONYM(S)
AFRL/RXLM

11. SPONSORING/MONITORING AGENCY REPORT NUMBER(S)
AFRL-RX-WP-TP-2011-4292

12. DISTRIBUTION/AVAILABILITY STATEMENT
Approved for public release; distribution unlimited.

13. SUPPLEMENTARY NOTES
PAO Case Number: 88ABW 2010-6751; Clearance Date: 03 Jan 2011. Document contains color.
Journal article submitted to the *Journal of Alloys and Compounds.*

14. ABSTRACT
A refractory alloy, $Ta_{20}Nb_{20}Hf_{20}Zr_{20}Ti_{20}$, was produced by vacuum arc-melting. The as-solidified alloy had a dendritic structure, which was not affected by hot isostatic pressing (HI Ping) conducted at T = 1200 °C and ρ = 207 MPa for 3 hours. The alloy had a single-phase body-centered cubic (BCC) structure with the lattice parameter a= 340.44 pm. The alloy density and Vickers microhardness after HIPing were ρ = 9.94 g/cm3 and *Hv* = 3826 MPa. Room temperature compression testing of HIPd samples revealed excellent ductility. The samples deformed homogeneously without any evidence of cracking at least up to 50% compression strain. Continuous strengthening followed yielding at 807 MPa. A simple model of solid-solution strengthening is proposed to explain the behavior.

15. SUBJECT TERMS
refractory alloy, $Ta_{20}Nb_{20}Hf_{20}Zr_{20}Ti_{20}$, vacuum arc-melting, hot isostatic pressing

16. SECURITY CLASSIFICATION OF:			17. LIMITATION OF ABSTRACT:	18. NUMBER OF PAGES	19a. NAME OF RESPONSIBLE PERSON (Monitor)
a. REPORT	b. ABSTRACT	c. THIS PAGE			Jonathan E. Spowart
Unclassified	Unclassified	Unclassified	SAR	24	19b. TELEPHONE NUMBER *(Include Area Code)* N/A

MICROSTRUCTURE AND ROOM TEMPERATURE PROPERTIES OF A HIGH-ENTROPY TaNbHfZrTi ALLOY

O.N. Senkov, [1,2,*] J.M. Scott, [1,2] S.V. Senkova, [1,2] D.B. Miracle [1] and C.F. Woodward [1]

[1] Air Force Research Laboratory, Materials and Manufacturing Directorate, Wright-Patterson Air Force Base, OH 45433, USA

[2] UES, Inc., Dayton, OH 45432, USA

ABSTRACT

A refractory alloy, $Ta_{20}Nb_{20}Hf_{20}Zr_{20}Ti_{20}$, was produced by vacuum arc-melting. The as-solidified alloy had a dendritic structure, which was not affected by hot isostatic pressing (HIPing) conducted at T = 1200 °C and P = 207 MPa for 3 hours. The alloy had a single-phase body-centered cubic (BCC) structure with the lattice parameter a = 340.44 pm. The alloy density and Vickers microhardness after HIPing were ρ = 9.94 g/cm^3 and H_v = 3826 MPa. Room temperature compression testing of HIPd samples revealed excellent ductility. The samples deformed homogeneously without any evidence of cracking at least up to 50% compression strain. Continuous strengthening followed yielding at 807 MPa. A simple model of solid-solution strengthening is proposed to explain the behavior.

1 INTRODUCTION

Metallic alloys with superior mechanical and functional properties remain in high demand for the aerospace industry. A recently proposed concept of multi-component high-entropy alloys opened up interesting possibilities in the alloy developments. According to this concept, that was proved experimentally on a number of compositions, high entropy of mixing can stabilize disordered solid solution phases and prevent formation of intermetallic phases during solidification, which may lead to alloys with high strength and good ductility. In order to achieve high entropy of mixing, the alloy must have typically five or more major elements of roughly equi-molar concentrations. Thus, while these alloys are compositionally complex, they are microstructurally simple. [1,2]

Two refractory high entropy alloys, $Ta_{25}Nb_{25}W_{25}Mo_{25}$ and $Ta_{20}Nb_{20}W_{20}Mo_{20}V_{20}$ were reported recently [3,4]. These alloys had a single-phase BCC structure and high Vickers hardness of 4.5

* Corresponding author. Phone: 937-2551320, e-mail: oleg.senkov@wpafb.af.mil

GPa and 5.3 GPa, respectively, as well as they showed very high yield strength ($\sigma_{0.2}$) values in the temperature range from room to 1600°C. For example, $\sigma_{0.2}$ of 405 MPa and 477 MPa at 1600°C were reported for the $Ta_{25}Nb_{25}W_{25}Mo_{25}$ and $Ta_{20}Nb_{20}W_{20}Mo_{20}V_{20}$ alloys, respectively. Unfortunately, these refractory alloys had high density (13.8 g/cm^3 for the four- and 12.4 g/cm^3 for the five-element alloy) and were practically brittle at room temperature. Moreover, presence of V accelerated oxidation of the $Ta_{20}Nb_{20}W_{20}Mo_{20}V_{20}$ alloy at high temperatures [5]. In this paper, we report results on development and characterization of a new refractory high entropy alloy (HEA), $Ta_{20}Nb_{20}Hf_{20}Zr_{20}Ti_{20}$. Replacement of heavier W, Mo and V with lighter Hf, Zr and Ti has been found to considerably decrease the alloy density and improve room temperature ductility.

2 EXPERIMENTAL PROCEDURES

The Ta-Nb-Hf-Zr-Ti alloy was prepared at the Air Force Research Laboratory by vacuum arc melting of the equimolar mixtures of the corresponding elements. Titanium, zirconium and hafnium were in the form of 3.175 mm diameter slugs with a purity of 99.98%, 99.95% and 99.9%, respectively. Niobium and tantalum were in the form of 1.0 and 2.0 mm wires, and their purity was 99.95% and 99.9%, respectively. High vacuum of 2.1×10^{-4} N/m^2 was achieved and high purity titanium was used as a getter for residual gases in the arc melting chamber prior the chamber was filled with the high purity argon of 5.1×10^{4} N/m^2. Arc melting of the alloy was conducted on a water-cooled copper plate. To achieve homogeneous distribution of elements in the alloy, it was re-melted three times, was flipped for each melt, and was in a liquid state for about 5 minutes during each melting event. The prepared button was about 8 mm thick and had shiny surfaces, indicating no oxidation during vacuum arc melting. The actual alloy composition obtained with the use of inductively-coupled plasma-optical emission spectroscopy (ICP-OES), is given in Table 1. The crystal structure was identified with the use of a Rigaku X-ray diffractometer, Cu Kα radiation, and the 2Θ range of 5° to 140°.

The density of the alloy was measured with an AccuPyc 1330 V1.03 pycnometer. The pycnometer cell volume was 12.2284 cm^3, the weight of the sample was ~10 g and was measured with accuracy of ±0.0001 g, and the volume of the samples was determined with the accuracy of ±0.0001 cm^3 by measurement of the free volume of the loaded cell using the helium gas and ten purges. Vickers microhardness was measured on polished cross-section surfaces

using a 136-degree Vickers diamond pyramid under 500 g load applied for 30 seconds. The microstructure was analyzed with the use of a scanning electron microscope (SEM) equipped with the backscatter electron (BSE) detector.

To close porosity presented in the as-solidified sample, it was hot isostatically pressed (HIPd). Prior to HIPing, the sample was wrapped with a 0.1 mm thick Ta foil, placed in a low carbon (1010) steel container with the wall thickness of 0.89 mm, and the container was vacuum sealed. The container was then placed in the HIP chamber and HIPd under the following conditions: heating at the constant rate of 10 °C/min to 1200 °C with a simultaneous increase in pressure to 207 MPa, holding at 1200°C / 207 MPa for 3 hours, cooling to room temperature at 20 °C/min with simultaneous pressure release.

Cylindrical specimens for compression testing were electric-discharge machined from the HIPd alloy. The specimen axis was perpendicular to the button surface, which was in contact with the copper plate during arc melting. The sample surfaces were mechanically polished and the compression faces of the samples were paralleled. The samples were 3.7 mm in diameter and ~ 5.6 mm in height. Compression tests to a 50% height reduction were conducted at room temperature and a constant ramp speed that corresponded to the initial strain rate of 0.001 s^{-1} in a computer-controlled Instron (Instron, Norwood, MA) mechanical testing machine outfitted with silicon carbide dies. A thin Teflon foil was used between the compression faces and silicon carbide dies to reduce friction. The deformation of the samples was video-recorded and an optical setup was used to measure strain versus load.

3 RESULTS

3.1 Crystal Structure, Alloy Density and Microhardness

Figure 1 shows the X-ray diffraction pattern of the cast and HIP'd alloy. All seven major diffraction peaks on this X-ray pattern have been identified to belong to a body centered cubic (BCC) phase and the indexes of the crystal planes corresponding to the X-ray diffraction peaks are shown in the figure. The lattice parameter of the BCC phase determined from this diffraction pattern is $a = 340.4 \pm 0.1$ pm. An additional low-intensity diffraction peak presented in the X-ray pattern at d = 357.8 pm indicates the presence of a minor secondary phase, which crystal structure and composition were not identified.

The density of the alloy in the solidified and HIP'd condition was determined to be ρ_I = 9.94 ± 0.01 g/cm^3. Vickers microhardness H_v of the alloy was measured in sixteen randomly selected locations and the average value is 3826 MPa. The scatter around the average microhardness value was ΔH_v = ±80 MPa.

3.4 Compression Properties

The engineering stress, S, vs. engineering strain, e, and true stress, σ, vs. true strain, ε, curves of the $Ta_{20}Nb_{20}Hf_{20}Zr_{20}Ti_{20}$ alloy obtained during compression testing at different temperatures are shown in Figure 2a and Figure 2b, respectively. The yield stress, $\sigma_{0.2}$, was 893±15 MPa. After yielding, the alloy showed continuous strengthening and the rate of an increase in S with e was almost constant, $\gamma = dS/de$ = 3360 MPa, while a parabolic-type strengthening, $\sigma = \sigma_{0.2}(\varepsilon_p/0.002)^{0.085}$, where ε_p is the true plastic strain, was observed for the true stress vs. true strain behavior.

3.5 Microstructure

Figure 3 illustrates a non-homogeneous microstructure of the $Ta_{20}Nb_{20}Hf_{20}Zr_{20}Ti_{20}$ alloy after solidification and HIPing. The microstructure at the bottom side, which was in a contact with the chill copper plate, consists of fine equiaxial dendritic grains. In accord to Z-contrast and EDS analysis, the dendrites were enriched with heavy elements, Ta and Nb, while the interdendritic regions were enriched with lighter elements, Zr and Ti. Hf was almost homogeneously distributed in the alloy. Equiaxed grains at the top side of the solidified and HIPd alloy were less segregated. The elements were more homogeneously distributed resulting in a less-pronounced Z contrast.

Figure 4 shows SEM backscatter images of a radial cross-section of a specimen compressed by 50% at room temperature. A rather uniform deformation, with a very small sample barreling and no evidence of strain localization, occurred (Figure 4a). Deformed grains that are elongated in the radial direction and the dendrite alignment in the same direction are clearly seen (Figure 4b). Higher magnification images reveal deformation twins and cracking along some grain boundaries (Figure 4c).

4 DISCUSSION

4.1 Crystal Structure and Alloy Density

The reported results indicate that, in spite of heavy alloying, the $Ta_{20}Nb_{20}Hf_{20}Zr_{20}Ti_{20}$ alloy has a single-phase BCC crystal structure, which remains stable after HIPing at 1200°C and furnace cooling to room temperature. The absence of extra-peaks from element ordering suggests random distribution of the elements in this BCC phase. It is necessary to point out that all five elements in the alloy have the BCC crystal lattices just below their melting temperatures and no intermetallic phases are present in binary systems of these elements [6]. The BCC structure of Ta and Nb retains down to room temperature, and the lattice parameters for these elements, determined at room temperature [7], are given in Table 2. The Ta-Nb binary system is a continuous solid solution within the entire composition range. Three other elements, Hf, Zr and Ti, also form continuous solid solutions with each other, but they exhibit polymorphic transformations and have a hexagonal close packed (HCP) crystal structure at room temperature. Reported BCC lattice parameters for these elements, a_{Hf} = 361.5 pm, a_{Zr} = 360.9 pm and a_{Ti} = 330.65 pm were determined at temperatures 1743°C, 867°C and 882°C, respectively [**Error! Bookmark not defined.**]. These values can however be extrapolated to room temperature by using reported coefficients of thermal expansion (CTE) for BCC Hf (9×10^{-6} K^{-1}), Zr (9×10^{-6} K^{-1}) and Ti (10.9×10^{-6} K^{-1}) [8]. Thus calculated room temperature BCC lattice parameters for these three elements are also given in Table 2.

Alloying of Hf, Zr and Ti with Ta and/or Nb is known to stabilize the high-temperature BCC phase and may result in a mixture of the BCC and HCP solid solution phases (or even a single BCC phase in the Ti alloys) at room temperature. Therefore, the presence of the single disordered BCC phase in the quinternary alloy, which contains 40 at.% of the BCC-stabilized elements, is expected. It is however not yet known if the BCC phase is thermodynamically stable at room temperature or it is metastable and formation of the low temperature HCP phase is kinetically restricted due to slow diffusivity of elements in the multicomponent alloys [1,2,9]. Additional study involving long-time annealing at temperatures below 600°C is required to answer this question.

Using rule of mixtures (i.e. Vegard's law [10]), one can calculate the 'theoretical' crystal lattice parameter a_{mix} of the disordered BCC solid solution:

$$a_{mix} = \sum c_i a_i \quad (1)$$

Here c_i is the atomic fraction of element i. The calculated (Calc) a_{mix} is given in Table 2. The experimental (Exp) a value, determined from the X-ray diffraction pattern is also given in this table. It can be seen that the calculated and experimental values of a are practically the same, which indicates that the lattice parameter of the alloy follows rule of mixtures. This analysis supports the X-ray results that the alloying elements are randomly distributed in the BCC phase. The theoretical density, ρ_{mix}, of a disordered solid solution is given by Equation (2):

$$\rho_{mix} = \frac{\sum c_i A_i}{\sum \frac{c_i A_i}{\rho_i}} \quad (2)$$

where A_i and ρ_i are the atomic weight and density of element i. The ρ_i values of the alloying elements taken from ref. [11] and the calculated ρ_{mix} value of the alloy (9,89 g/cc) are given in Table 3. It can be seen that the calculated density is about 0.50% smaller than the experimentally determined density of the alloy (9.94 g/cc). This very small difference can be due to different factors. First, the ρ values used for Hf, Zr and Ti belong to the HCP phase, while the density of the BCC polymorph of these elements extrapolated to room temperature should be used. These BCC polymorph densities can be estimated from the calculated lattice parameters given in Table 2 and are 13.15 g/cc, 6.59 g/cc and 4.52 g/cc for Hf, Zr, and Ti, respectively. It can be seen that the density of BCC Zr and Ti are indeed slightly higher than the density of the respective HCP phase. However, the estimated density of the BCC phase for Hf is slightly smaller than the density of HCP phase. Using these estimated density values for BCC Hf, Zr, and Ti, the corrected alloy density becomes 9.90 g/cc, which is still slightly below the experimentally determined density. Secondly, experimental errors in determining the alloy composition can also contribute to the difference. We may thus conclude that the alloy density follows the rule of mixtures, which is also in agreement with the random (disordered) distribution of the alloying elements in the BCC lattice of the alloy.

4.2 Room Temperature Mechanical Properties

The room temperature yield stress and Vickers microhardness of the HIP'd $Ta_{20}Nb_{20}Hf_{20}Zr_{20}Ti_{20}$ alloy are $\sigma_{0.2}$ = 893 MPa and Hv = 3826 MPa, which gives the hardness to stress ratio ϕ = Hv/$\sigma_{0.2}$ = 4.28. This is noticeably higher than the value ϕ = 3, which was predicted theoretically and observed experimentally for non-strain hardening materials (e.g. after cold working) [12]. Taber [12, p. 175] has noticed that ϕ = 3 also holds for pure metals and commercial alloys, regardless of the initial state of strain hardening, if the engineering stress S_8 corresponding to the engineering strain e ~ 8%, which is the average plastic strain for a Vickers indenter, is used instead of $\sigma_{0.2}$. Using the engineering stress vs. engineering strain curve (see Figure 2a), S_8 = 1270 MPa is obtained at e = 8%. This indeed gives the value ϕ_8 = Hv/S_8 = 3.0. One may therefore conclude that the high hardness to yield stress ratio observed for the studied high-entropy alloy is caused by its strain hardening during indentation.

The microhardness and the yield stress of the $Ta_{20}Nb_{20}Hf_{20}Zr_{20}Ti_{20}$ alloy do not follow the rule of mixtures of the respective properties of the constituent elements. Indeed, Table 4 shows typical H_v [13] and $\sigma_{0.2}$ [14] values for pure elements at room temperature. Using rule of mixtures, the 'theoretical' microhardness, $(H_v)_{mix} = \sum c_i H_{vi}$, and yield stress, $(\sigma_{0.2})_{mix} = \sum c_i \sigma_{0.2i}$, of the alloy were calculated. These values (Calc) are given in Table 4, together with the respective experimental (Exp) values. The calculated microhardness (1165 MPa) and yield stress ($\sigma_{0.2}{}^0$ = 226 MPa) of the alloy are much smaller than the respective experimental H_v and $\sigma_{0.2}$ values. The high microhardness and yield stress of the alloy are likely originated from solid solution-like strengthening.

It is widely accepted that the solid solution strengthening of metallic solid solutions arises from the elastic interactions between the local stress fields of solute atoms and those of dislocations [15,16,171819,]. The magnitude of the interaction force between a moving dislocation and the substitutional solid solutions, f_m, increases with an increase in both the atomic size misfit parameter, δ_a, and the modulus misfit parameter, δ_G, of the solute and solvent atoms:

$$f_m = Gb^2\delta = Gb^2[\delta_G + \beta\delta_a]. \quad (3)$$

Here $\delta_G = (1/G)dG/dc$, $\delta_a = (1/a)da/dc$, G is the shear modulus of the alloy, b is the magnitude of the Burgers vector, and β is a constant, which value depends on the type of the mobile dislocation. Generally, β is 2-4 for the screw dislocations and ≥ 16 for edge dislocations [15,17]. In a concentrated solid solution, the solute-induced stress increase, $\Delta\sigma$, can be expressed as a function of f_m, solute concentration, c, and dislocation line tension, E_L, [16,20]:

$$\Delta\sigma = A f_m^{4/3} c^{2/3} E_L^{-1/3} \quad (4)$$

Here A is a dimensionless material constant. Using an expression $E_L = Gb^2/2$ and combining Equations (3) and (4), the following equation for $\Delta\sigma$ is obtained [21]:

$$\Delta\sigma = A' G \delta^{4/3} c^{2/3} \quad (5)$$

where A' is a material-dependent dimensionless constant, which is of the order of 0.1 [16]. Unfortunately, the mechanisms of solid solution strengthening were developed for conventional solid solutions, in which the concentration of the matrix element (solvent) exceeds 60-70%, and these mechanisms may not be applicable to high-entropy alloys, where all elements are at almost the same atomic concentrations (≤ 20%) and multiple element interactions are expected. Nevertheless, an attempt to estimate the effects of the atomic size (lattice) and shear modulus distortions on the dislocation force, f_m, in the HEA will be given below.

Each solute in the BCC crystal lattice has 8 nearest-neighbor atoms, thus forming a 9-atom cluster. In the diluted alloys with no solute interactions, the neighbors are all solvent atoms and the local lattice distortions near the solute are caused by the atomic size and modulus mismatches between the solute and the solvent atoms. In the heavily alloyed multi-component alloy, on the other hand, an i element can neighbor with different elements and the lattice distortion near this element is now a function of the atomic size and modulus mismatches between this element and all its nearest neighbors. The local environment around each element can roughly be estimated if we assume that the local concentration is equal to the average concentration of the alloy. For example, in the 5-element alloy with equimolar concentrations, an element i will have, in average, 1.8 atoms of each of the other elements and 0.8 atoms of the same element. Then the

lattice distortion δ_{ai} in the vicinity of an element *i* is estimated as an average of the atomic size difference of this element with its neighbors:

$$\delta_{ai} = \frac{9}{8}\sum c_j \delta_{aij} \quad (6)$$

Here c_j is the atomic fraction of a *j* element in the alloy, 9 is the number of atoms in the *i*-centered cluster in the BCC lattice, 8 is the number of atoms neighboring with the center atom *i*, and $\delta_{aij} = 2(r_i - r_j)/(r_i + r_j)$ is the atomic size difference of elements *i* and *j*.

Similarly, the modulus distortion, δ_{Gi}, in the vicinity of an element *i* is estimated as

$$\delta_{Gi} = \frac{9}{8}\sum c_j \delta_{Gij} \quad (7)$$

where $\delta_{Gij} = 2(G_i - G_j)/(G_i + G_j)$.

The atomic radii and shear moduli of the alloying elements are given in Table 5, while the calculated δ_{aij} and δ_{Gij} values are given in Table 6. Using these values and Equations (6) and (7), the lattice- and modulus- distortions near each element in the $Ta_{20}Nb_{20}Hf_{20}Zr_{20}Ti_{20}$ solid solution alloy were calculated and the results are given in Table 7.

The data in Table 6 shows that the pairs of Hf and Zr elements, as well as the pairs of Ta, Nb and Ti elements, have very little atomic size difference, $\delta_{aij} \leq 0.008$. On the other hand, the size difference of Hf and Zr with three other elements is at least one order of magnitude higher ($\delta_{aij} \approx 0.08$). The absolute values of the estimated lattice distortions near each element (see Table 7) are of the same order ($|\delta_{ai}| \sim 0.04$-0.06). As it is expected, smaller elements, Ta, Nb and Ti, produce local tension strains ($\delta_{ai} \sim -0.04$), while larger elements, Hf and Zr, produce local compression strains ($\delta_{ai} \sim 0.05$). To roughly estimate the contribution of the lattice distortion to f_m and $\Delta\sigma$, we may consider the alloy as a pseudo-binary solid solution, with Ta, Nb and Ti as the solvents and 40at.% of Hf plus Zr as the solutes, which produce the lattice distortion $\delta_a \sim 0.09$. By assigning $G = 40$ GPa, $b = 197$ pm, $\beta = 2$, ignoring for now the modulus distortion contribution and using Equations 3 and 5 one can estimate $f_{ma} \approx 2.8\times10^{-10}$ N and $\Delta\sigma_a \approx 221$ MPa. Here subscript '*a*' indicates the lattice distortion contribution.

The elastic modulus difference of the alloying elements has a wide spectrum of values, from δ_{Gij} = 0.10 for the Hf-Zr atom pair to 0.79 for Ta-Hf atom pair (Table 6). Pairing of Ta atoms with other elements provides the strongest shear modulus effect (δ_{Gij} values are in the range from 0.44 for Ta-Ti to 0.79 for Ta-Hf), while Hf-Zr and Nb-Zr pairs resulted in smaller δ_{Gij} values of 0.10 and 0.14, respectively. The calculated modulus distortions near a particular element in the BCC lattice of the alloy, δ_{Gi}, also have the largest values of δ_{Gi} = 0.57 near Ta atoms (Table 7). Assuming that the modulus mismatch contributions to the interaction force f_{mG} and stress increase $\Delta\sigma_a$ is mainly due to Ta, these contributions are estimated to be $f_{mG} \approx 8.8\times10^{-10}$ N and $\Delta\sigma_a \approx 647$ MPa.

The estimated values for f_{ma} and f_{mG} are of the same order of magnitude as those reported for binary solid solutions [20]. This very rough analysis of the contributions of the atomic size and modulus difference to the yield stress of the alloy predicts $\sigma_{0.2} = \sigma_{0.2}^{0} + \Delta\sigma_a + \Delta\sigma_G = 1094$ MPa, which is about 35% higher than the experimentally observed $\sigma_{0.2}$ = 807 MPa, which can be considered as a good agreement. Indeed, the model does not take into account thermally activated processes, which should ease the deformation processes and reduce the stress. The good ductility of the alloy at room temperature is probably due to simultaneous dislocation and twin activity, which effectively reduce stress localization along grain boundaries. It is apparent that the grain boundaries are the weakest structural elements along which cracks eventually develop after heavy deformation.

5 CONCLUSIONS

A refractory alloy, $Ta_{20}Nb_{20}Hf_{20}Zr_{20}Ti_{20}$, produced by vacuum arc-melting, has a single-phase body-centered cubic (BCC) structure with the lattice parameter a = 340.44 pm. No phase changes occur after HIPing the alloy at 1200°C, 207 MPa for 3 hours. The alloy density and Vickers microhardness after HIPing were ρ = 9.94 g/cm^3 and H_v = 3826 MPa. The alloy has high compression yield stress ($\sigma_{0.2}$ = 892 MPa) and ductility (ε >50%). The alloy shows considerable strengthening and homogeneous deformation. The high stress is explained by solid-solution strengthening.

ACKNOWLEDGEMENTS

Discussions with Drs. G. Wilks, S. Rao, D. Dimiduk, P. Martin, F. Meisenkothen, and R. Wheeler are recognized. This work was supported through the Air Force Office of Scientific Research (Dr. Ali Sayir, Program Manager) and through the USAF Contract No. FA8650-10-D-5226.

TABLES

Table 1. Chemical composition of the TaNbHfZrTi alloy produced by vacuum arc melting.

Composition	Ta	Nb	Hf	Zr	Ti
At. %	19.68	18.93	20.46	21.23	19.7
Wt. %	30.04	14.84	30.82	16.34	7.96

Table 2. The lattice parameter, *a*, of the BCC crystal structure of the pure metals and the studied alloy at room temperature. For Hf, Zr and Ti, the parameter *a* was extrapolated from elevated temperatures (see section 3.1 for details).

Metal	Ta	Nb	Hf	Zr	Ti	Alloy Calc	Alloy Exp
a, pm	330.3	330.1	355.9	358.2	327.6	340.9	340.4

Table 3. Density of pure metals and the studied TaNbHfZrTi alloy. Both calculated (Calc, using Eq. 2) and experimental (Exp) values are shown for the alloy.

Metal	Ta	Nb	Hf	Zr	Ti	Alloy Calc	Alloy Exp	$\Delta\rho/\rho$ $\times 100\%$
ρ, g/cm^3	16.65	8.57	13.31	6.51	4.51	9.89	9.94	0.60

Table 4. Vickers microhardness, H_v, and yield stress, $\sigma_{0.2}$, values of pure metals and the TaNbHfZrTi alloy at room temperature. Both the calculated (Calc.) and experimental (Exp) values are shown for the alloy.

Metal	Ta	Nb	Hf	Zr	Ti	Alloy Calc	Alloy Exp
H_v, MPa	873	1320	1760	903	970	1165	3826
$\sigma_{0.2}$, MPa	170	240	240	280	195	226	807

Table 5. Atomic radius, $r = a/\sqrt{3}$, and shear modulus, G, of pure elements.

Element/Property	Ta	Nb	Hf	Zr	Ti
r, pm	143.0	142.9	154.1	155.1	141.8
G, MPa	69	38	30	33	44

Table 6. Relative atomic size difference, δ_{aij} (underlined numbers), and modulus difference, δ_{Gij} (bold numbers), of the alloying elements.

Element i\j $\underline{\delta_{aij}}$ \ $\boldsymbol{\delta_{Gij}}$	Ta	Nb	Hf	Zr	Ti
Ta		**0.58**	**0.79**	**0.71**	**0.44**
Nb	<u>0.00</u>		**0.24**	**0.14**	**-0.15**
Hf	<u>0.07</u>	<u>0.08</u>		**-0.10**	**-0.38**
Zr	<u>0.08</u>	<u>0.08</u>	<u>0.01</u>		**-0.29**
Ti	-<u>0.01</u>	-<u>0.01</u>	-<u>0.08</u>	-<u>0.09</u>	

Table 7. Calculated lattice distortion, δ_{ai}, and modulus distortion, δ_{Gi}, (Equations 6 and 7) near each element in the BCC lattice of the TaNbHfZrTi alloy.

Element	Ta	Nb	Hf	Zr	Ti
δ_{ai}	-0.035	-0.035	0.049	0.057	-0.044
δ_{Gi}	0.571	-0.073	-0.331	-0.228	0.089

FIGURES

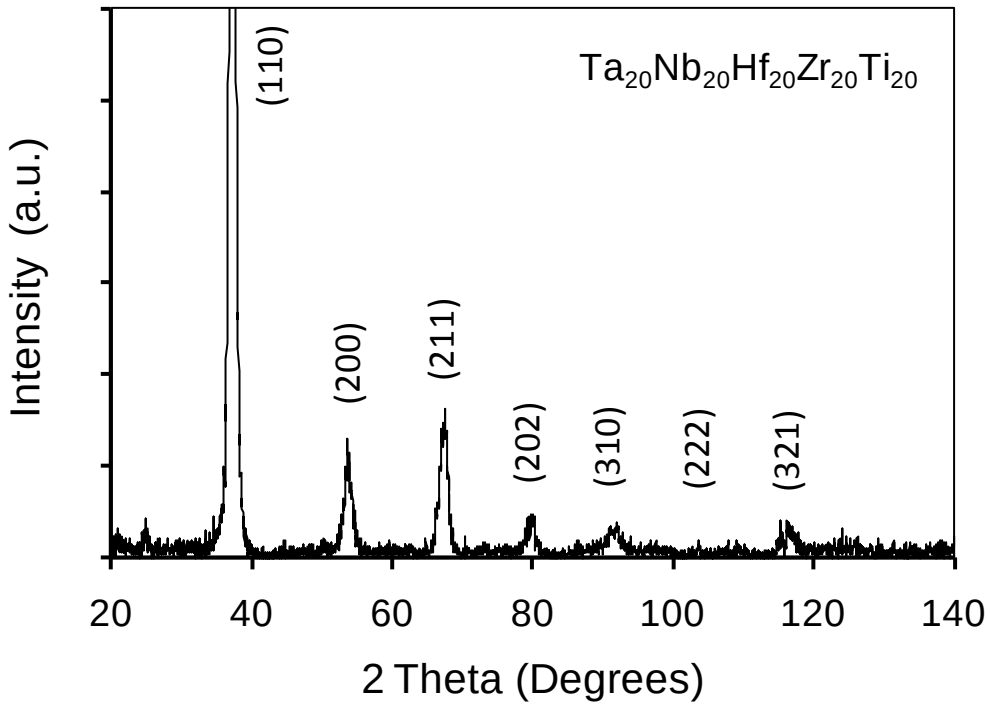

Figure 1. X-ray diffraction pattern of the TaNbHfZrTi alloy. The indexed peaks belong to a BCC crystal lattice with the lattice parameter a = 340.4 pm.

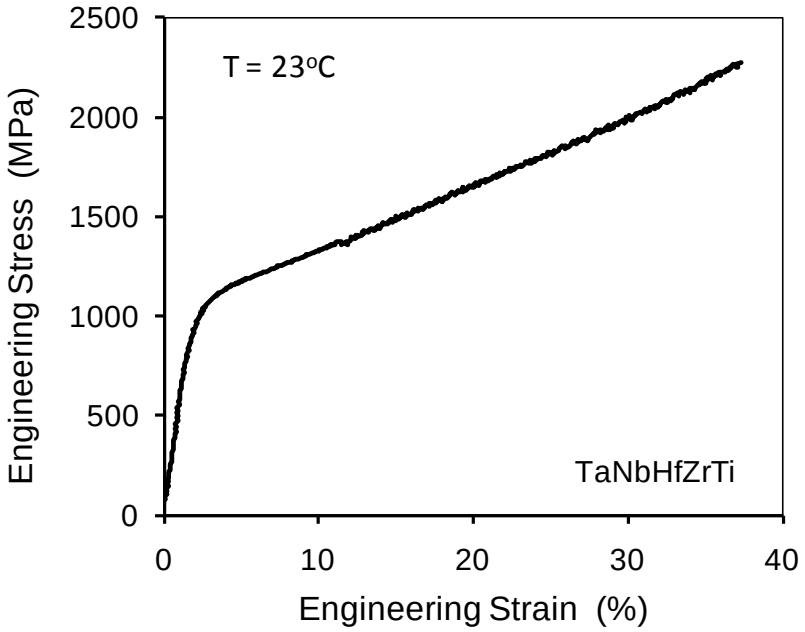

(a)

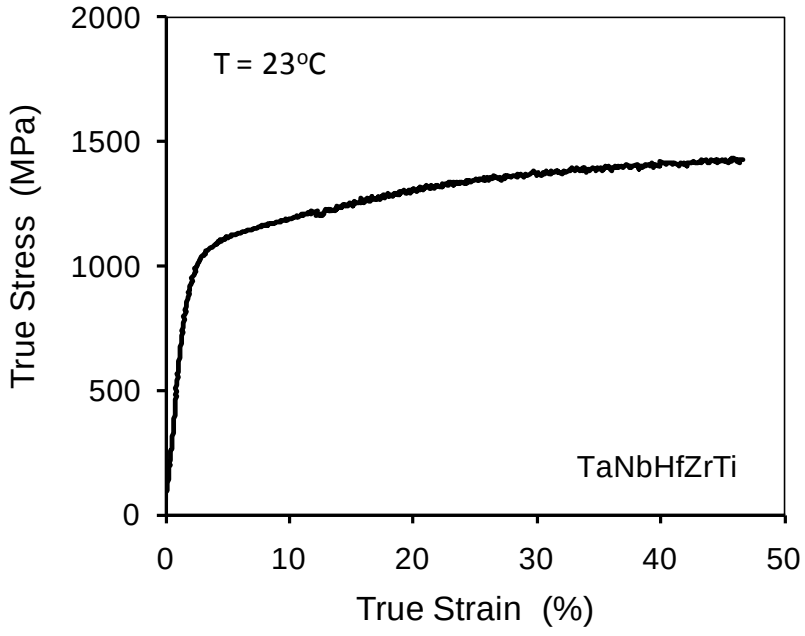

(b)

Figure 2. (a) Engineering stress vs. engineering strain and (b) true stress vs. true strain compression curves of the $Ta_{20}Nb_{20}Hf_{20}Zr_{20}Ti_{20}$ alloy at different temperatures.

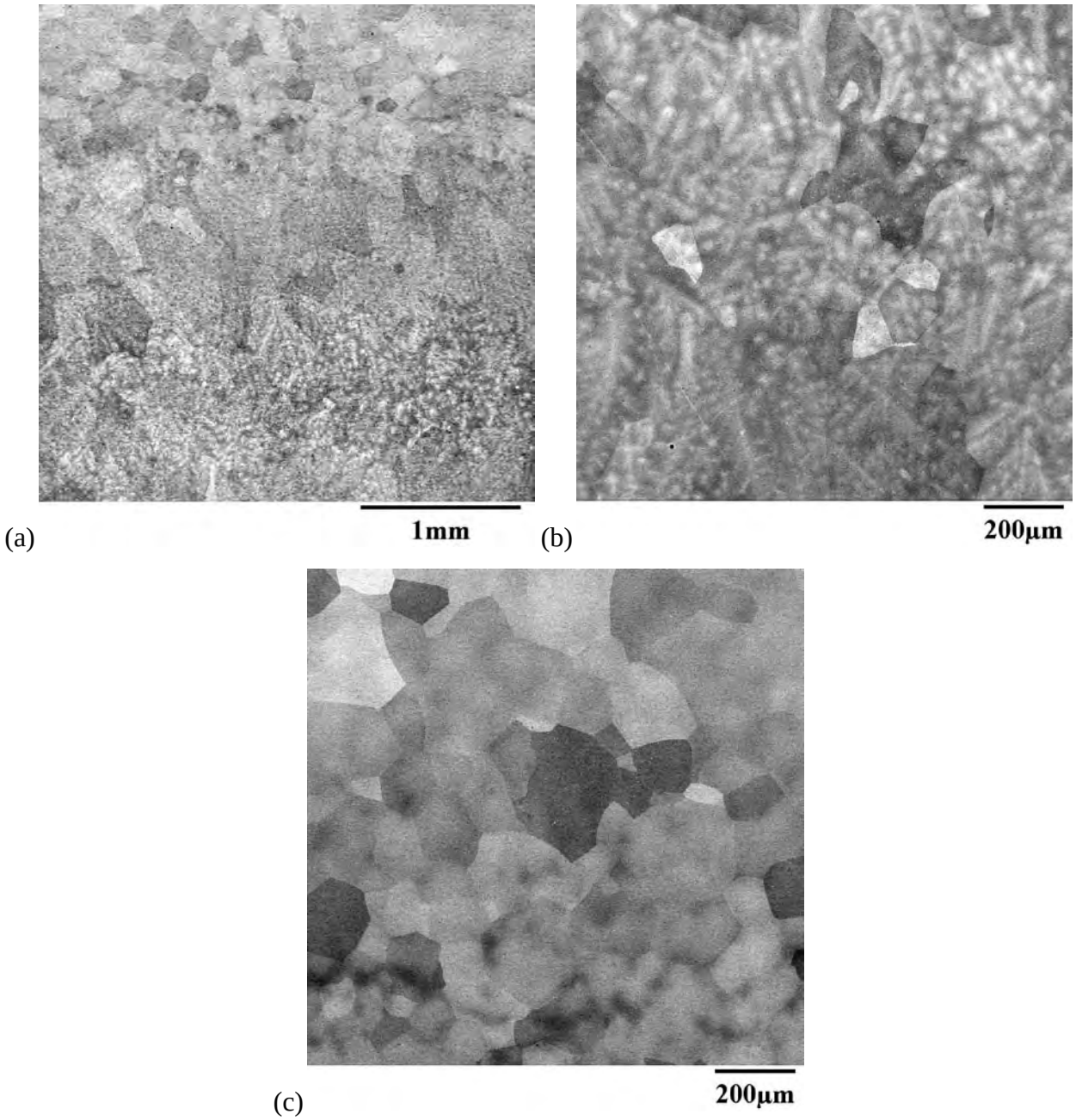

(a) (b) (c)

Figure 3. SEM backscatter electron images of a polished cross-section of the arc-melted and HIP'd $Ta_{20}Nb_{20}Hf_{20}Zr_{20}Ti_{20}$ alloy. (a) A low magnification image shows a non-homogeneous dendritic and grain structure of the solidified alloy. (b) and (c) are higher magnification images of the bottom and top sides of the alloy.

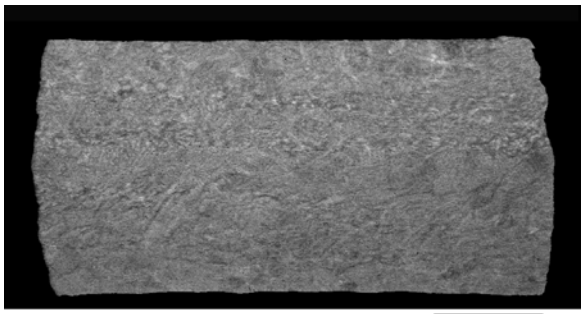

(a)

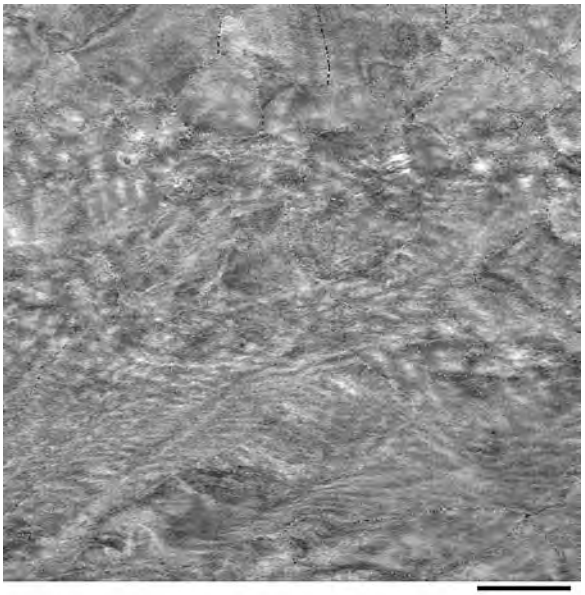

(b)

(c)

Figure 4. SEM backscatter images of a radial cross-section of a specimen after 60% compression at 23°C.

REFERENCES

1 J.-W. Yeh, Annales de Chimie: Science des Materiaux, 31 (2006) 633-648.

2 J.-W. Yeh, Y.-L. Chen, S.-J. Lin, S.-K. Chen, Mater. Sci. Forum, 560 (2007) 1-9.

3 O.N. Senkov, G.B. Wilks, D.B. Miracle, C.P. Chuang, P.K. Liaw, Intermetallics, 18 (2010) 1758-1765.

4 O.N. Senkov, G.B. Wilks, J.M. Scott, D.B. Miracle, Intermetallics, submitted in 2010.

5 O.N. Senkov, G.B. Wilks, D.B. Miracle, Refractory High Entropy Alloys: Microstructure and Properties, Unpublished presentation, May 2010.

6 T.B. Massalski, H. Okamoto, P.R. Subramanian, L. Kacprzak, Binary Alloy Phase Diagrams, 2nd Ed., ASM Internat., Materials Park, OH, USA, 1990.

7 International Tables for X-ray Crystallography, Birmingham, England, 1968;

8 M. Chase, JANAF Thermochemical Tables, 3rd Ed., J. Phys. Chem. Ref. Data, 1985; J.D. Cox, CODATA Key Values for Thermodynamics, Hemisphere Publ. Co., NY 1989; A.T. Dinsdale, SGTE Data for Pure Elements, CALPHAD, 15 (4) (1991) 317-425.

9 M.-H. Tsai, J.-W. Yeh, J.-Y. Gan, Thin Solid Films, 516 (2008) 5527-5530.

10 L. Vegard, Zeitschrift fur Physik, 5 (1021) 17-26.

11 WebElements: http://www.webelements.com/periodicity/density.

12 D. Taber, The Hardness of Metals, Oxford University Press, London, 1951.

13 Hardnesses of the elements:
http://en.wikipedia.org/wiki/Hardnesses_of_the_elements_(data_page)

14 Goodfellow, Index of Materials: http://www.goodfellow.com/E/T.html

15 R.L. Fleischer, Acta met. 11 (1963) 203-209.

16 R. Labusch, Acta Metall. 20 (1972) 917; Phys. Stat. Sol. 41 (1970) 659.

17 L.A. Gypen, A. Deruyttere, J. Mater. Sci. 12(1977) 1028-1033.

18 T. Suzuki, Jap. J. Appl. Phys. 20 (1981) 449-462.

19 C. Meyers, *Mechanical Behavior of Materials.* Cambridge University Press, UK, 1999.

20 H. Mughrabi (Vol. Ed.), Materials Science and Technology, Vol. 6: Plastic Deformation and Fracture of Materials, VCH, Cambridge, 1993, pp. 191-250.

21 R.J. Arsenault (Ed.) Treatise on Materials Science and Technology, Vol. 6: Plastic Deformation of Materials, Acad. Press, New York, 1975, p. 1-99.